Article

EMBO reports

A subpopulation of itch-sensing neurons marked by Ret and somatostatin expression

Kalina K Stantcheva[1], Loredana Iovino[1,2], Rahul Dhandapani[1], Concepcion Martinez[1], Laura Castaldi[1], Linda Nocchi[1], Emerald Perlas[1], Carla Portulano[1], Martina Pesaresi[1], Kalyanee S Shirlekar[1], Fernanda de Castro Reis[1], Triantafillos Paparountas[3], Daniel Bilbao[1] & Paul A Heppenstall[1,2,*]

Abstract

Itch, the unpleasant sensation that elicits a desire to scratch, is mediated by specific subtypes of cutaneous sensory neuron. Here, we identify a subpopulation of itch-sensing neurons based on their expression of the receptor tyrosine kinase Ret. We apply flow cytometry to isolate Ret-positive neurons from dorsal root ganglia and detected a distinct population marked by low levels of Ret and absence of isolectin B4 binding. We determine the transcriptional profile of these neurons and demonstrate that they express neuropeptides such as somatostatin (Sst), the NGF receptor TrkA, and multiple transcripts associated with itch. We validate the selective expression of Sst using an Sst-Cre driver line and ablated these neurons by generating mice in which the diphtheria toxin receptor is conditionally expressed from the sensory neuron-specific *Avil* locus. Sst-Cre::Avil^{iDTR} mice display normal nociceptive responses to thermal and mechanical stimuli. However, scratching behavior evoked by interleukin-31 (IL-31) or agonist at the 5HT$_{1F}$ receptor is significantly reduced. Our data provide a molecular signature for a subpopulation of neurons activated by multiple pruritogens.

Keywords DRG; sensory neurons; IL-31; 5HT$_{1F}$
Subject Category Neuroscience
DOI 10.15252/embr.201540983 | Received 7 July 2015 | Revised 22 January 2016 | Accepted 26 January 2016 | Published online 29 February 2016
EMBO Reports (2016) 17: 585–600

Introduction

The perception of physical and chemical stimuli through the skin is initiated by peripheral sensory neurons that have their cell body in the DRG. The complexity of somatosensation is reflected by the fact that a myriad of sensations including touch, pain, itch, and temperature are recognized by the peripheral nervous system. It has long been debated whether this functional complexity arises from activation of specific subtypes of sensory neuron for each stimulus modality, or from encoding and summation of neuronal activity generated by neurons that can detect a broad range of stimuli [1]. Recently, it has been proposed that the sensation of itch is a discrete sensory modality that utilizes a dedicated neuronal pathway tuned to perceive only this sensation [2–4].

Itch, the sensation that elicits a desire to scratch, serves a protective function against potentially harmful environmental irritants [5]. Although unpleasant, itch is inherently different from pain, both in its sensory quality and its behavioral outcome (scratching compared to withdrawal). The neuronal pathways that mediate itch versus pain also appear to be distinct. In the spinal cord, ablation of neurons expressing receptors for the neuropeptides, gastrin-releasing peptide (Grp) [4] or natriuretic polypeptide b (Nppb) [3], reduces itch responses to multiple pruritogens but does not affect nociceptive behavior. Similarly, subpopulations of C-fiber primary afferents are activated by pruritogens [6–8] and ablation or selective activation of DRG neurons positive for the Mas-related G protein-coupled receptor A3 (MrgprA3) impacts upon scratching behavior but not pain [2].

Itch is further categorized by its dependence upon histaminergic or non-histaminergic mechanisms. Histamine-dependent itch is elicited through activation of the H1 receptor (HRH1) and signaling through phospholipase-β3 (PLCβ3) and the ion channel TRPV1 [9,10]. The existence of further histamine-independent pathways is supported by observations that many chronic pruritic syndromes such as atopic dermatitis are resistant to antihistamine therapy [11]. Mechanistically, histamine-independent itch is likely to be mediated by activation of the ion channel TRPA1. For example, injection of the antimalarial agent chloroquine induces itch [12] via MrgprA3 receptors [13] functionally coupled to TRPA1 [14], and TRPA1 is also required for itch produced by oxidative stress and leukocyte accumulation [15,16]. Other antihistamine-resistant itch responses include those elicited by cytokines such as interleukin-31 (IL-31) released from T cells during allergic itch [17,18]. IL-31 induces severe pruritus and may be a key mediator in atopic dermatitis [19].

Further information of the molecular profile of itch-sensing neurons and identification of molecular markers for different subtypes of itch neuron would be valuable for understanding how

1 EMBL Mouse Biology Unit, Monterotondo, Italy
2 Molecular Medicine Partnership Unit (MMPU), Heidelberg, Germany
3 IRCCS Santa Lucia, Rome, Italy
*Corresponding author. Tel: +39 690091233; Fax: +39 690091272; E-mail: paul.heppenstall@embl.it

different pruritogens activate itch pathways. Intriguingly, a recent study which took an unbiased approach to classify sensory neuron subtypes identified three populations of putative itch receptors [20]. Each of these populations was enriched for transcripts associated with itch. However, from their gene expression profile, it was not clear whether they all signal only itch or can also contribute to other sensations such as pain.

To distinguish different populations of sensory neuron and ultimately define their function, we examined the expression pattern of the glial-derived neurotrophic factor (GDNF) receptor Ret in mouse DRG. Almost every DRG neuron expresses at least one neurotrophic factor [21], and approximately 60 percent of cells are marked by Ret [22]. The Ret tyrosine kinase is the signaling receptor for GDNF family ligands GDNF, neurturin, artemin, and persephin which bind via GPI-anchored co-receptors termed GFRα1–4 to initiate signaling through Ret [23]. Two distinct waves of Ret expression arise during development with the first occurring prior to E11.5 and the second emerging subsequently [22,24]. Early Ret-positive neurons develop into rapidly adapting mechanoreceptors and express the co-receptor GFRα2 and high levels of Ret [25,26]. Late Ret-positive neurons form a large heterogeneous group of non-peptidergic nociceptors that can be distinguished by their binding of the plant lectin IB4 [22,24]. A further population of Ret-positive neuron co-expresses the enzyme tyrosine hydroxylase (TH) [27,28] and forms C-fiber low threshold mechanoreceptors which have been implicated in the affective component of touch [29]. Finally, a fourth population of Ret-positive neurons that expresses the neurotrophin receptor TrkA in adult mice has also been described [22,30]. This population is rare, corresponding to around 10% of all Ret cells, and its role *in vivo* is unknown.

We sought to determine the function of this unique population of Ret-positive sensory neuron. To this end, we took a genetic approach and generated mice where eGFP expression was driven from the *Ret* locus exclusively in peripheral sensory neurons [31,32]. We identified multiple subpopulations of Ret-positive neurons in DRG which were quantified using flow cytometry. Microarray analysis of Ret-expressing neurons that were negative for IB4 uncovered a sparse population of cells enriched in transcripts for TrkA, neuropeptides such as somatostatin (Sst), and pruritogen receptors. We validated the expression of Sst in this population using an Sst-Cre driver line and generated a new mouse line to selectively ablate these neurons *in vivo*. Mice displayed normal nociceptive responses to thermal and mechanical stimuli. However, scratching behavior evoked by several classes of pruritogen was significantly reduced. Thus, Ret marks a population of itch receptors characterized by their co-expression of Sst and multiple pruritogen receptors.

Results

Ret-eGFP expression in primary sensory neurons

To examine Ret expression in the adult peripheral nervous system, $Ret^{eGFP/+}$ mice [31] were crossed with $Avil^{cre/+}$ [32] mice to obtain heterozygote Avil-Cre::$Ret^{eGFP/+}$ mice. This approach allowed us to target all DRG neurons and avoid extraneous GFP expression in surrounding tissues. Heterozygous mice were viable, exhibited no overt behavioral phenotype, and displayed robust eGFP fluorescence in peripheral sensory ganglia.

We investigated Ret-eGFP distribution in DRG by co-staining sections from Avil-Cre::$Ret^{eGFP/+}$ mice with a selection of markers for different subtypes of sensory neuron. Ret-eGFP was present in 55 percent of neurons (Fig 1M) and displayed a broad range of fluorescence intensities across different cells. We examined expression with IB4 and NF200, markers of non-peptidergic nociceptors and myelinated neurons, respectively, and observed overlap with the majority of Ret-eGFP-positive neurons (Fig 1A–D), reflecting the early and late Ret neurons described previously [22,24]. We further investigated Ret-eGFP co-expression with TH, a marker of C-fiber low threshold mechanoreceptors [27,28]. eGFP fluorescence was evident in many TH-positive neurons and these cells were not co-labeled with NF200 or IB4 (Fig 1E–L). Our analysis also indicated that a small proportion of Ret-eGFP-positive neurons were not marked by either IB4, NF200, or TH, suggesting the existence of a novel subtype of Ret-expressing neuron. We quantified the overlap between Ret-eGFP and each marker and determined that 14% of Ret-eGFP-positive neurons were negative for all markers (Fig 1N), supporting the idea that this population may reflect a functionally uncharacterized subset of primary afferent neuron.

We utilized Avil-Cre-driven Ret-eGFP expression to examine the peripheral and central projections of Ret-positive sensory neurons. In the skin, Ret-eGFP fluorescence was broadly distributed and present in free nerve endings terminating in the dermis and epidermis (Appendix Fig S1), and in lanceolate endings encircling hairs (Appendix Fig S1). Similarly in spinal cord sections, Ret-eGFP was widely expressed across the dorsal horn. This was evident as a dense plexus of expression in lamina II_o corresponding to IB4-positive non-peptidergic nociceptors (Appendix Fig S2) and more diffusely through laminae III to V overlapping with NF200-labeled mechanoreceptor inputs (Appendix Fig S2). Notably, we also detected Ret-eGFP expression immediately ventral to IB4-positive terminals that coincided with PKCγ, a marker for lamina II_i/III interneurons (Appendix Fig S2), and in lamina I co-expressed with CGRP. Thus, RET-eGFP expression distinguishes multiple populations of peripheral sensory neuron that are likely to be functionally distinct.

To obtain quantitative data on the distribution of Ret-positive neuronal populations in DRG, we applied flow cytometric analysis to acutely dissociated neurons. We focused on levels of IB4 binding and native Ret-eGFP fluorescence as this would allow for quantitative measurements in live cells. In line with histological data, we observed both IB4-positive and IB4-negative populations of Ret-eGFP neuron (Figs 2A and EV1). Importantly, however, flow cytometric analysis revealed multiple well-defined subpopulations delineated by their levels of eGFP fluorescence and IB4 binding (termed Ret-$eGFP^{Lo}$:$IB4^{Neg}$ (A), Ret-$eGFP^{Hi}$:$IB4^{Neg}$ (B), Ret-$eGFP^{Lo}$:$IB4^{Lo}$ (C), Ret-$eGFP^{Hi}$:$IB4^{Lo}$ (D), and Ret-$eGFP^{Hi}$:$IB4^{Hi}$ (E)). There was a broad distribution in cell size across all populations as determined by forward scatter values, and no correlation between size and levels of IB4 binding or fluorescence (Fig 2B). We further validated flow cytometric analysis using fluorescent microscopy and observed that in both sensory neuron cultures (Fig 2C) and sections of DRG (Fig 2D) from Avil-Cre::$Ret^{eGFP/+}$ mice, native eGFP fluorescence varied by an order of magnitude across IB4-positive and IB4-negative cells.

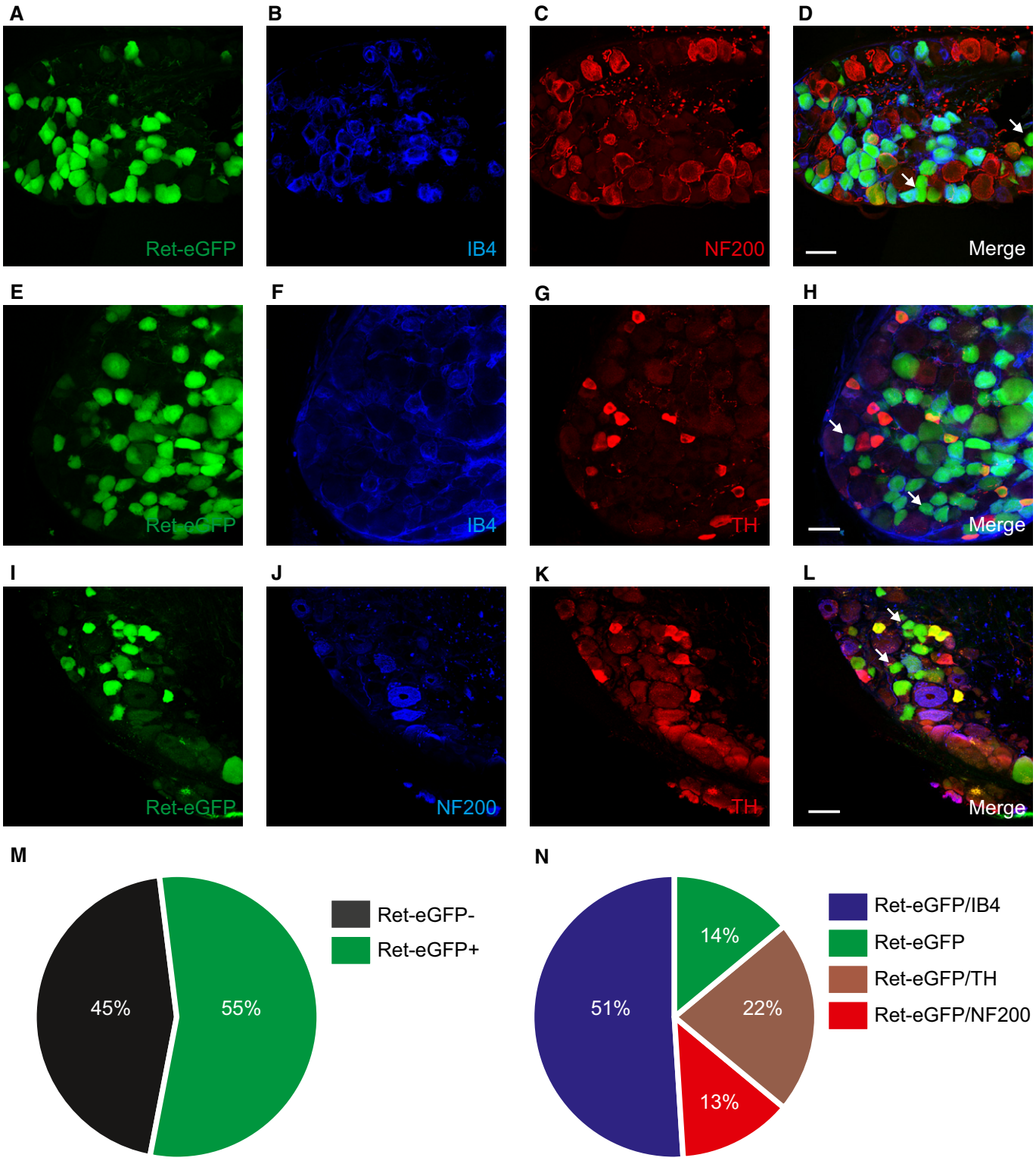

Figure 1. Ret-eGFP is expressed in multiple sensory neuron subsets.

A–L Ret-positive neurons largely overlap with markers for myelinated neurons (NF200), non-peptidergic nociceptors (IB4), and C-fiber low threshold mechanoreceptors (TH). However, some Ret-positive neurons are negative for these markers (indicated by the arrows in D, H, and L) suggesting the existence of a further subset of Ret^+ neurons. Scale bars, 50 μm.

M Quantification of the proportion of Ret-eGFP-positive neurons in DRG (n = 2,278 cells from three mice).

N Quantification of Ret-eGFP co-expression with other markers (n = 2,278 cells from three mice).

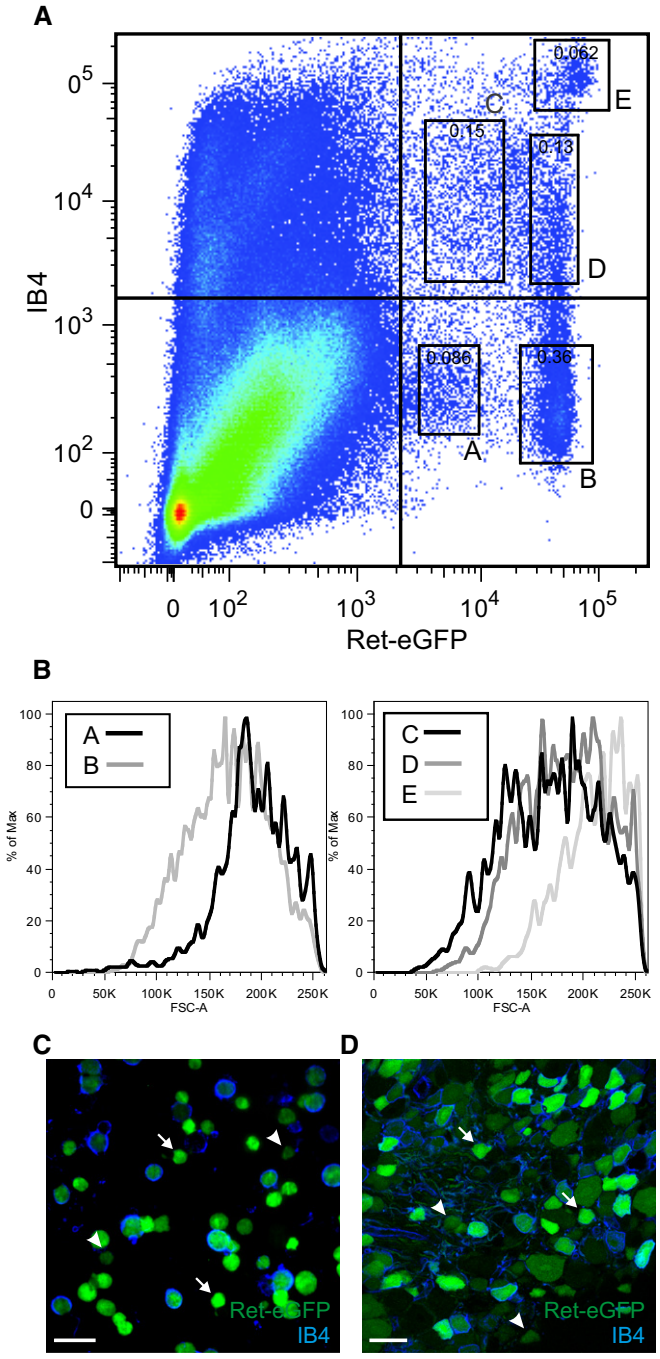

Figure 2. Multiple Ret-positive subpopulations as determined by flow cytometric analysis of dissociated sensory neurons from Avil-Cre::Ret$^{+/eGFP}$ mice.

A Flow cytometric analysis of dissociated sensory neurons plotted according to their level of endogenous Ret-eGFP expression and IB4 binding (also indicated in Fig EV1). There are 5 well-defined subsets, 2 of which do not bind to IB4 but display a differential level of eGFP intensity (termed Ret-eGFP^{Lo}:IB4^{Neg}, A, and Ret-eGFP^{Hi}:IB4^{Neg}, B, respectively). The other 3 subsets bind IB4 and display a range of eGFP intensities, termed Ret-eGFP^{Lo}:IB4^{Lo}, C, Ret-eGFP^{Hi}:IB4^{Lo}, D, and Ret-eGFP^{Hi}:IB4^{Hi}, E. Percent of total events are indicated in each box.

B No correlation between the median cell size of different Ret^{+} subsets and eGFP intensity or IB4 binding. The graph shows the forward scatter values plotted against the normalized number of cells, displayed as the percent of Max.

C, D Variations in endogenous eGFP intensity are clearly visible with fluorescent microscopy. (C) Cultured neurons and (D) DRG section from Avil-Cre::Ret$^{+/eGFP}$ mice displaying native eGFP fluorescence and stained with IB4. Different levels of eGFP intensity (high, indicated by arrows, and low, indicated by arrowheads) are detected across IB4^{+} and IB4^{-} cells. Scale bar, 50 μm.

Transcription profiling of Ret-eGFP- and IB4-negative neurons

We reasoned that by defining the molecular composition of Ret-eGFP populations, we may be able to gain clues as to their function. We focused on IB4-negative neurons because flow cytometric data indicated that these cells formed two well-defined and potentially homogeneous populations. Moreover, while one of these populations presumably corresponds to RA mechanoreceptors [25,26], the other may reflect an as yet uncharacterized population of Ret-positive neurons. We performed differential microarray screening on sorted Ret-eGFP^{Hi}:IB4^{Neg} and Ret-eGFP^{Lo}:IB4^{Neg} cells and determined that these two populations do indeed cluster into distinct, homogeneous subsets. We further identified several functional markers in each population that gave a first indication as to their identity. For example, Ret-eGFP^{Lo}:IB4^{Neg} cells were enriched in transcripts for TRPV1, CGRP (Calca), and the Ret co-receptors GFRα1 and GFRα3 (Fig 3A), while Ret-eGFP^{Hi}:IB4^{Neg} neurons expressed significantly higher levels of Ret, GFRα2, and the mechanosensitive ion channel Piezo 2 (Fam38b) (Fig 3A). Intriguingly, neither population was enriched for TH. We thus speculate that Ret-eGFP^{Hi}:IB4^{Neg} neurons may correspond to RA mechanoreceptors, while Ret-eGFP^{Lo}:IB4^{Neg} cells represent a novel, functionally distinct subtype of nociceptor.

We sought to define the function of the novel Ret-eGFP^{Lo}:IB4^{Neg} population and observed that this subset was highly enriched in molecules previously implicated in itch (Fig 3A, red dots). For example, transcripts for histamine-dependent itch mediators HRH1, PLCβ3, and TRPV1 were all differentially expressed in Ret-eGFP^{Lo}:IB4^{Neg} neurons, as were itch-associated neurotransmitters such as Nppb [3] and neuromedin B (Nmb) [33], and the co-receptors for IL-31, Il31ra, and Osmr. However, other molecules implicated in itch such as GRP, MrgprC11, and endothelin receptors were not over-expressed in Ret-eGFP^{Lo}:IB4^{Neg} neurons, suggesting that these cells may contribute to a subtype of itch receptor.

To further investigate whether itch-associated receptor transcripts were indeed specifically expressed in Ret-eGFP^{Lo}:IB4^{Neg} neuron, we performed a second microarray screen where we assessed differential expression in this population with respect to all DRG neurons. We sorted DRG neurons from Avil-Cre::R26^{tdRFP} mice in which the majority of peripheral sensory neurons are marked by RFP fluorescence (Appendix Fig S3) and subjected them to microarray analysis. Similar to differential screening between Ret-eGFP^{Lo}:IB4^{Neg} and Ret-eGFP^{Hi}:IB4^{Neg} populations, this dataset was also enriched in itch-associated molecules (Fig 3B). Fold change levels were lower than for comparisons with Ret-eGFP^{Hi}:IB4^{Neg} neurons (Fig 3C), presumably reflecting the mixed molecular profile of all DRG neurons, and the fact that some transcripts such as Calca (CGRP) mark large populations of Ret-negative neurons.

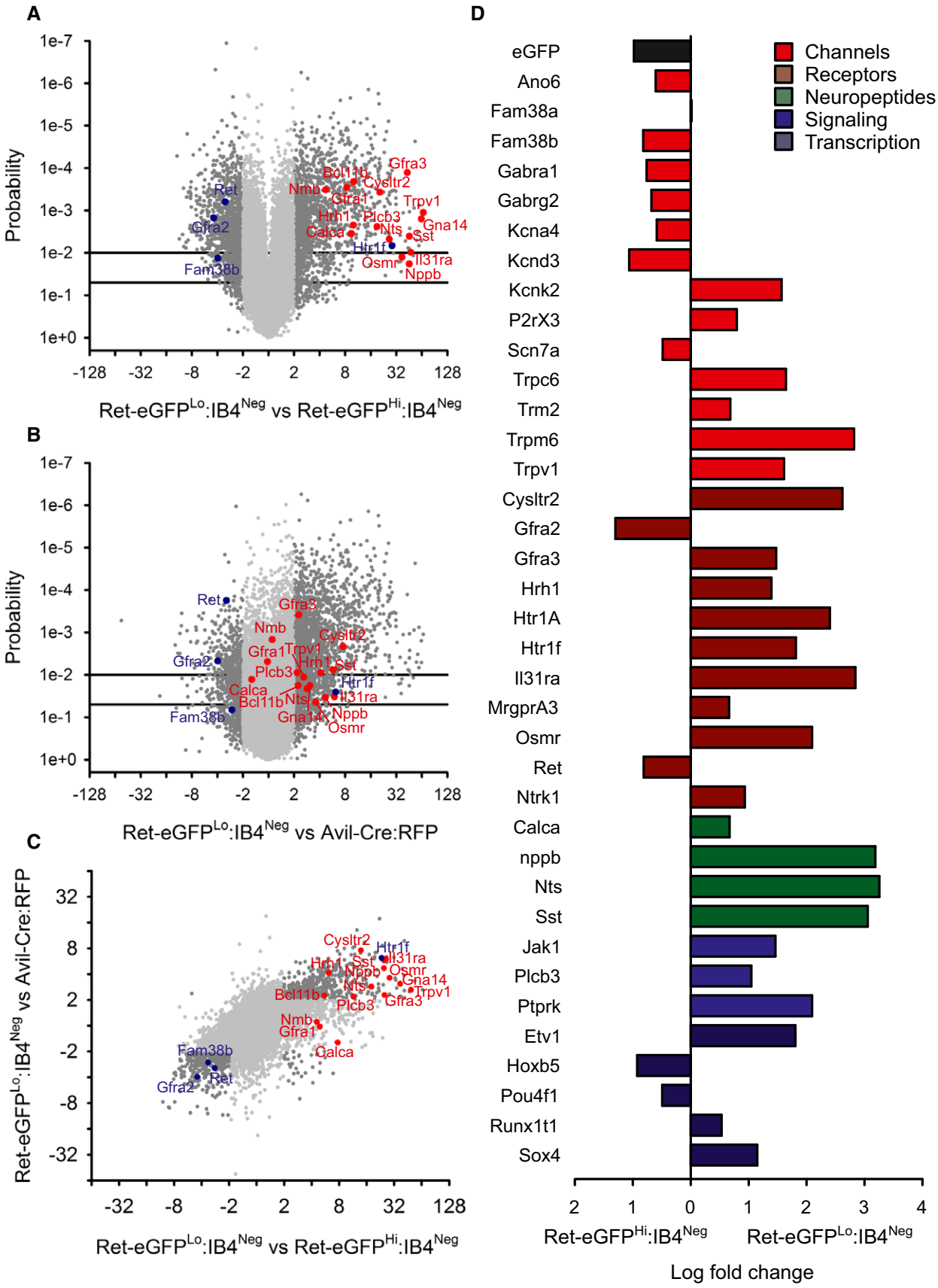
A
Probability
1e-7
1e-6
1e-5
1e-4
1e-3
1e-2
1e-1
1e+0
-128 -32 -8 -2 2 8 32 128
Ret-eGFP^Lo:IB4^Neg vs Ret-eGFP^Hi:IB4^Neg
Ret
Gfra2
Fam38b
Bcl11b
Nmb
Cysltr2
Gfra3
Gfra1
Trpv1
Hrh1
Plcb3
Gna14
Calca
Nts
Sst
Htr1f
Osmr
Il31ra
Nppb
B
Probability
Ret-eGFP^Lo:IB4^Neg vs Avil-Cre:RFP
C
Ret-eGFP^Lo:IB4^Neg vs Avil-Cre:RFP
32
8
2
-2
-8
-32
Ret-eGFP^Lo:IB4^Neg vs Ret-eGFP^Hi:IB4^Neg
D
eGFP
Ano6
Fam38a
Fam38b
Gabra1
Gabrg2
Kcna4
Kcnd3
Kcnk2
P2rX3
Scn7a
Trpc6
Trm2
Trpm6
Trpv1
Cysltr2
Gfra2
Gfra3
Hrh1
Htr1A
Htr1f
Il31ra
MrgprA3
Osmr
Ret
Ntrk1
Calca
nppb
Nts
Sst
Jak1
Plcb3
Ptprk
Etv1
Hoxb5
Pou4f1
Runx1t1
Sox4
Channels
Receptors
Neuropeptides
Signaling
Transcription
2 1 0 1 2 3 4
Ret-eGFP^Hi:IB4^Neg
Ret-eGFP^Lo:IB4^Neg
Log fold change

Figure 3.

Figure 3. Transcriptional profiling of Ret-eGFP^{Hi}:IB4^{Neg} and Ret-eGFP^{Lo}:IB4^{Neg} sensory neurons.

A Ret-eGFP^{Hi}:IB4^{Neg} and Ret-eGFP^{Lo}:IB4^{Neg} neurons display distinct expression profiles. A volcano plot of fold change expression in Ret-eGFP^{Lo}:IB4^{Neg} versus Ret-eGFP^{Hi}:IB4^{Neg} against probability. Ret has higher expression in the Ret-eGFP^{Hi}:IB4^{Neg} subset, which also shows an upregulation of the Ret co-receptor Gfra2 and Fam38b, encoding for the mechanosensitive ion channel Piezo 2. The Ret-eGFP^{Lo}:IB4^{Neg} subset displays an array of molecules previously associated with itch (marked in red).

B Itch-associated transcripts are enriched in the Ret-eGFP^{Lo}:IB4^{Neg} population compared to all DRG neurons. Volcano plot of fold change expression in Ret-eGFP^{Lo}:IB4^{Neg} neurons versus sorted neurons from Avil-Cre::R26^{tdRFP} mice against probability. Molecules linked to itch perception are significantly upregulated in the Ret-eGFP^{Lo}:IB4^{Neg} subset.

C Gene expression within the Ret-eGFP^{Lo}:IB4^{Neg} population is confirmed by triple comparison between Ret-eGFP^{Lo}:IB4^{Neg}, Ret-eGFP^{Hi}:IB4^{Neg}, and Avil-Cre::R26^{tdRFP} datasets.

D Validation of differential microarray screening by quantitative RT–PCR. Transcripts encoding ion channels, receptors, neuropeptides, signaling molecules, and transcription factors were selected for quantitative RT–PCR. Differential expression between Ret-eGFP^{Lo}:IB4^{Neg} and Ret-eGFP^{Hi}:IB4^{Neg} populations correlates with microarray analysis (n = 3).

To validate the microarray analysis, we performed parallel quantitative RT–PCR analysis of 38 transcripts in Ret-eGFP^{Lo}:IB4^{Neg} and Ret-eGFP^{Hi}:IB4^{Neg} populations using a microfluidic platform (Fluidigm). We selected genes that represented not only itch-associated transcripts but also ion channels, signaling molecules, and transcription factors with a demonstrated role in the peripheral nervous system. In agreement with microarray data, high differential expression between Ret-eGFP^{Lo}:IB4^{Neg} and Ret-eGFP^{Hi}:IB4^{Neg} neurons was evident for itch-related genes such as the neuropeptide Nppb, the membrane receptors Il31ra, Osmr, Cysltr2, MrgprA3, and Hrh1, and the signaling molecule Plcb3. We also observed higher expression in this population for other markers such as Ntrk1 (TrkA), Calca (CGRP), and Trpv1 transcripts, marking it as a novel population of Ret-positive neurons, as well as the ion channels Trpm6, Trpc6, Trpm2, and P2rx3 and the serotonin receptors Htr1f and Htr1a (Fig 3D and Appendix Fig S4). In the Ret-eGFP^{Hi}:IB4^{Neg} population, we detected almost 10-fold higher expression of Ret and eGFP, validating the flow cytometry analysis. In addition, Gfra2 and the mechanosensitive ion channel Piezo 2 (Fam38b) (but not Piezo 1 (Fam38a)) were upregulated, supporting the assumption that these neurons function as RA mechanoreceptors. Intriguingly, we also observed that this population was enriched in transcripts involved in chloride transport including the GABA channel subunits α1 and γ2 (Gabra1, Gabrg2) and the putative chloride channel anoctamin 6 (Ano6) (Fig 3D and Appendix Fig S4).

Sst^{Cre} as a surrogate marker for Ret-eGFP^{Lo}:IB4^{Neg} neurons

In order to investigate the function of Ret-eGFP^{Lo}:IB4^{Neg} neurons, we required a molecular tool with which to selectively manipulate this population. From the microarray and quantitative RT–PCR analysis, the neuropeptide somatostatin (Sst) was among the highest enriched transcripts in Ret-eGFP^{Lo}:IB4^{Neg} cells, displaying a 1,126-fold higher expression compared to the Ret-eGFP^{Hi}:IB4^{Neg} population. Moreover, an Sst^{Cre} driver line is available which has been well characterized in the CNS [34]. We thus examined the expression pattern of Sst^{Cre}-mediated recombination in the PNS to determine whether it coincides with the Ret-eGFP^{Lo}:IB4^{Neg} population and could be used to genetically target these cells.

We first assessed the anatomical properties of Sst^{Cre}-positive neurons by crossing the Sst^{Cre} driver line with Ret^{eGFP} mice to generate heterozygote Sst-Cre::Ret$^{eGFP/+}$ mice. In DRG sections from these animals, we detected weak eGFP fluorescence in a sparse population of cells corresponding to 1.3% of all neurons (Fig 4I). We explored this expression pattern in more detail by co-staining sections with IB4, NF200, and TH (Fig 4A–H). Sst^{Cre}-driven Ret-eGFP expression was most evident in neurons not expressing any of these markers (85% of all Ret-eGFP-positive cells, Fig 4J), suggesting that Sst^{Cre} may indeed mediate recombination in the Ret-eGFP^{Lo}:IB4^{Neg} population.

To investigate whether Sst^{Cre} is selective for Ret-eGFP^{Lo}:IB4^{Neg} neurons, we crossed mice with a ubiquitous RFP reporter driven from the *Rosa26* locus (Sst-Cre::Rosa26^{RFP} mice) and performed immunohistochemistry for neuronal markers on DRG sections. We again observed a low number of RFP-positive cells (1.8% of total neurons, Fig EV2) that were mostly negative for IB4 and NF200 (87% of all Rosa26^{RFP}-positive cells, Fig EV2). These values were not significantly different from the number of Sst-Cre::Ret^{eGFP}-positive neurons (P = 0.36 for total cells and P = 0.7 for marker negative cells) implying that Sst^{Cre} does not drive substantial recombination beyond the Ret-eGFP^{Lo}:IB4^{Neg} population.

We further examined the peripheral projections of Sst^{Cre}-positive sensory neurons using a Rosa26^{SNAPCaaX} reporter mouse line that allows for highly sensitive detection of Cre-positive cells [35]. We labeled skin from Sst-Cre::Rosa26^{SNAPCaax} mice with fluorescent TMR-Star SNAP substrate and observed prominent fluorescence mainly confined to neurons that formed free nerve endings and ran parallel to the dermal/epidermal border of the skin (Fig 4K–M). In occasional sections, we also detected a rare population of hair follicles that were innervated by Sst^{Cre}-positive neurons (1.9 ± 1% of hair follicles in 3 out of 13 sections, Fig EV2). Importantly, this staining pattern was absent from skin taken from control mice not expressing Sst^{Cre}.

To obtain a more quantitative assessment of the degree of intersection between Sst^{Cre}-positive neurons and the Ret-eGFP^{Lo}:IB4^{Neg} population, we applied flow cytometric analysis to acutely dissociated neurons from Sst-Cre::Ret-eGFP mice. We followed an identical preparation protocol to that performed previously for Avil-Cre::Ret^{eGFP} mice and used the same gates for analysis. In line with histological data, we observed very few IB4-positive cells among the Sst-Cre::Ret^{eGFP} population, and furthermore, native GFP fluorescence was low (Fig 5A). Indeed, when comparing this data directly to flow cytometric analysis of Avil-Cre::Ret^{eGFP} neurons (Fig 5B), it was apparent that four out of the five subpopulations defined in earlier experiments were absent in Sst^{Cre} mice and only the Ret-eGFP^{Lo}:IB4^{Neg} was present.

Finally, we sought to validate the identity of Sst^{Cre}-positive sensory neurons by assessing their molecular composition compared to Ret-eGFP^{Lo}:IB4^{Neg} cells. We sorted Sst-Cre::Ret^{eGFP} cells using the same gating paradigm as described previously and

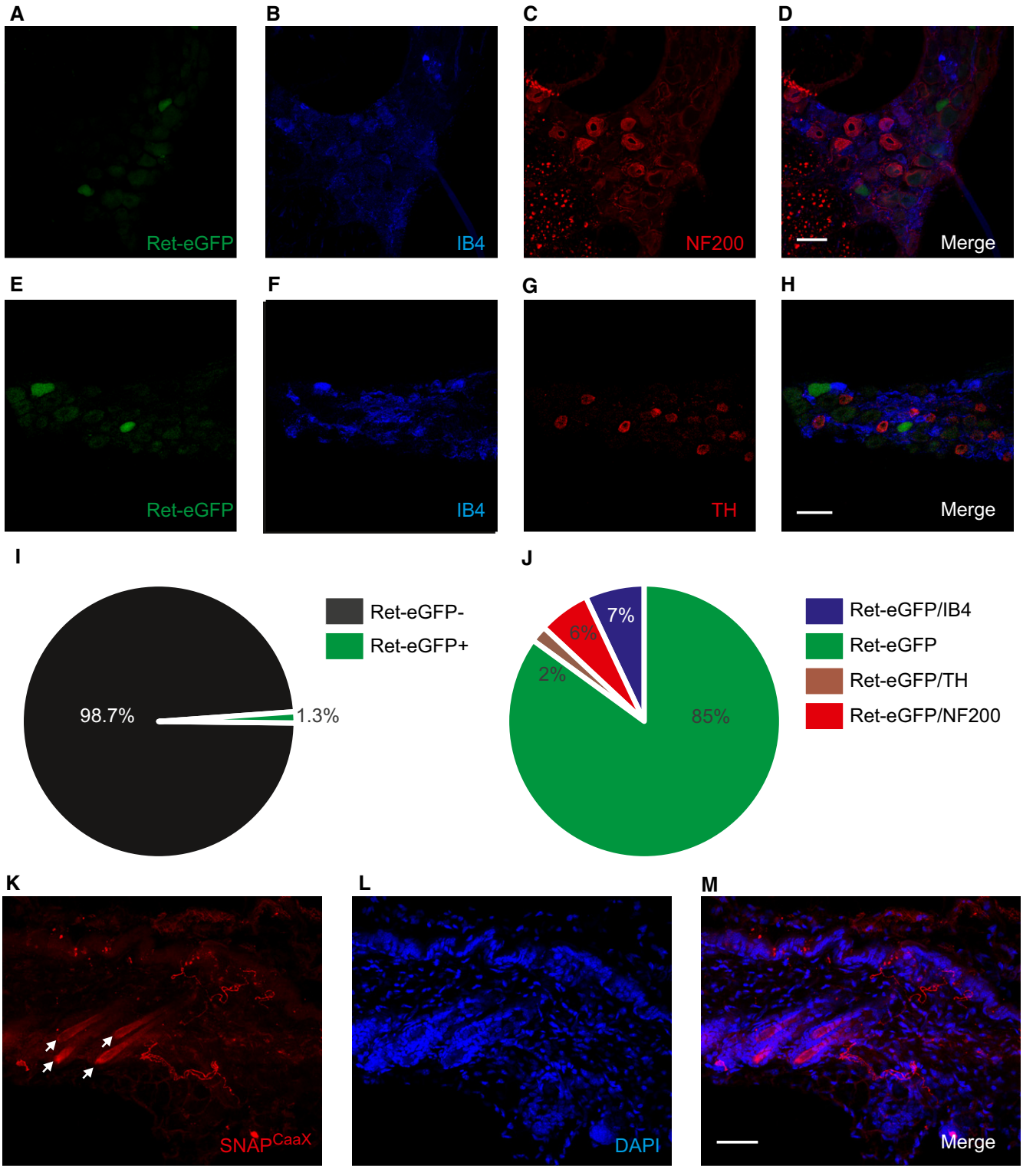

Figure 4. Sst^{Cre}-driven expression in DRG and skin.

A–H Sst^{Cre}-mediated recombination of the *Ret* locus drives eGFP expression in sensory neurons that do not bind to IB4 or co-express NF200 or TH. Triple immunostaining of DRG from Sst-Cre::$Ret^{eGFP/+}$ mice with RetGFP (A), IB4 (B), NF200 (C), RetGFP (E), IB4 (F), and TH (G). Scale bars, 50 μm.

I Quantification of Sst^{Cre}::Ret-eGFP expression in DRG (n = 8,827 cells from three mice).

J Quantification of co-expression of Sst^{Cre}::Ret-eGFP with neuronal markers (n = 8,827 cells from three mice).

K–M Peripheral projections of sensory neurons from Sst-Cre::$Rosa26^{SnapCaaX}$ mice terminate in the hairy skin as free nerve endings. Non-innervated hair follicles are indicated by arrows. Double labeling using TMR-Star to label SNAP tag (K) and DAPI (L). Scale bars, 50 μm.

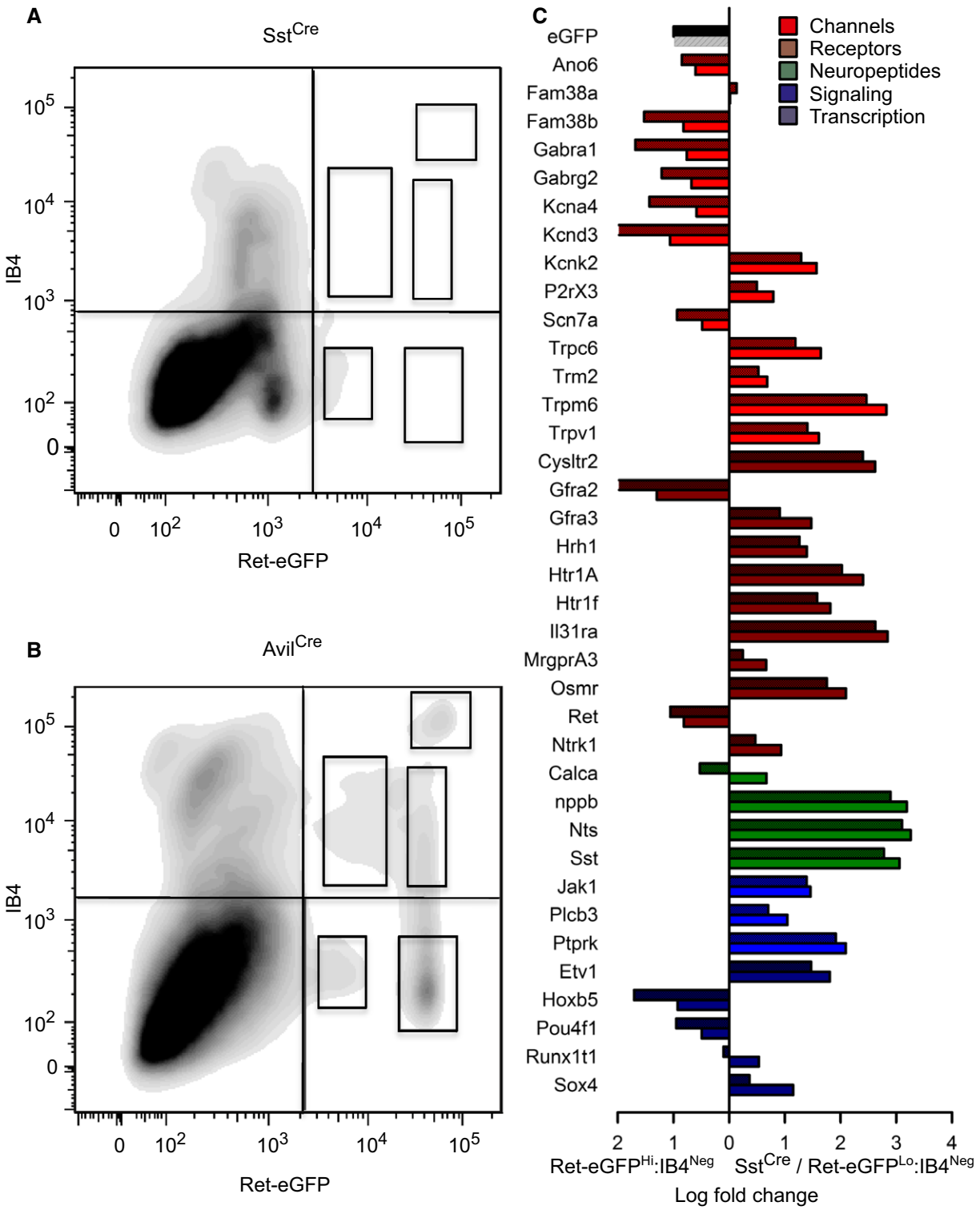

Figure 5. Flow cytometric and transcriptome analysis of Sst-Cre::Ret^{eGFP} versus Ret-eGFP^{Hi}:IB4^{Neg} sensory neurons.

A, B Contour diagram of dissociated sensory neurons from Sst-Cre::Ret$^{eGFP/+}$ (A) and Avil-Cre::Ret$^{eGFP/+}$neurons (B), plotted according to their native eGFP expression and IB4 binding. Only one subset of Ret-eGFP cells can be defined within the Sst-Cre::Ret$^{eGFP/+}$-dissociated DRG neurons. This displays the same range of eGFP fluorescence as the Ret-eGFP^{Lo}:IB4^{Neg} population and does not bind to IB4.

C Quantitative RT–PCR analysis of selected transcripts in the Sst-Cre::Ret^{eGFP} (darker colors) and Ret-eGFP^{Hi}:IB4^{Neg} (lighter colors) subsets displayed as differential expression compared to the Ret-eGFP^{Hi}:IB4^{Neg} subset. Almost all the genes that are upregulated in the Ret-eGFP^{Lo}:IB4^{Neg} compared to the Ret-eGFP^{Hi}:IB4^{Neg} subset are also enriched in the Sst-Cre::Ret^{eGFP} population (n = 3).

subjected cells to quantitative RT–PCR analysis. Strikingly, 36 out of 38 transcripts were regulated in the same direction as Ret-eGFP^{Lo}:IB4^{Neg} relative to Ret-eGFP^{Hi}:IB4^{Neg} cells (Fig 5C and Appendix Fig S5). Furthermore, levels of enrichment for both populations were remarkably similar, especially for the markers eGFP and Ret, and for itch-associated transcripts such as Hrh1, Il31ra, Osmr, Cysltr2, Plcb3, and Nppb (Fig 5C and Appendix Fig S5). Collectively, these data imply that Sst^{Cre} does indeed mark the Ret-eGFP^{Lo}:IB4^{Neg} population and that this population is largely homogenous.

Functional characterization of Sst^{Cre} neurons

To examine the function of Sst^{Cre}-positive neurons, we reasoned that selective ablation of this population could uncover their role in driving distinct somatosensory behaviors. A well-described and effective method for selectively ablating neurons *in vivo* involves Cre-dependent expression of the diphtheria toxin receptor from the *Rosa26* locus and subsequent treatment of animals with diphtheria toxin [36]. However, because Sst^{Cre} is expressed widely in the central nervous system [34], this approach would not be suitable for deleting only Sst^{Cre}-positive neurons in the peripheral nervous system. We thus generated a new mouse line where diphtheria toxin receptor is integrated into the sensory neuron-specific *Avil* locus preceded by a *loxP*-flanked stop cassette. Crossing these mice with a Cre driver line should therefore induce expression of the diphtheria toxin receptor only in peripheral sensory neurons, regardless of whether Cre is expressed in other tissues.

Avil^{iDTR} mice were generated using standard techniques for knock-in to the *Avil* locus (Fig EV3). Mice were healthy, displayed normal fertility, and did not exhibit any obvious defects. To assess Sst^{Cre}-mediated recombination of the Avil^{iDTR} transgene, Sst^{Cre} mice were crossed with Avil^{iDTR} animals to produce heterozygote Sst-Cre::Avil$^{iDTR/+}$ mice, and expression of the diphtheria toxin receptor determined using immunohistochemistry. In control Avil^{iDTR} mice (without the Cre), we detected no diphtheria toxin receptor expression. However, in mice with the Sst^{Cre} allele, a small number of diphtheria toxin receptor-positive cells were evident in DRG that was also negative for IB4 (Fig 6A–C and G). We next investigated the efficiency of ablation of these cells by applying diphtheria toxin systemically in mice and evaluating the number of diphtheria toxin receptor cells using immunohistochemistry. We observed an almost complete loss of diphtheria toxin receptor immunoreactivity after toxin application (Fig 6D–F). To determine whether ablation also impacts upon endogenous Sst expression and does not affect other populations, we performed immunocytochemistry on dissociated DRG neurons plated on glass coverslips and labeled with Sst and NF200 antibodies, and IB4. Sst-Cre::Avil$^{iDTR/+}$ mice treated with diphtheria toxin displayed a complete loss of Sst immunoreactivity with no change in the number of NF200- or IB4-positive neurons (Fig EV4). Finally, we carried out quantitative RT–PCR on Sst and other transcripts associated with the Ret-eGFP^{Lo}:IB4^{Neg} population (Hrh1, MrgprA3, Il31ra, and Htr1f). All transcripts were strongly downregulated upon diphtheria toxin-mediated ablation (Fig EV4), indicating that this strategy is an effective means of eliminating the Sst^{Cre} population *in vivo*.

To explore the function of Sst^{Cre}-positive cells, we initially performed calcium imaging on acutely dissociated DRG and investigated their activation by pruritogens. Based upon transcriptome analysis, we selected four receptor classes highly enriched in this population encompassing histamine-dependent (histamine) and histamine-independent signaling (chloroquine and IL-31), and a class of receptor, $5HT_{1F}$ not previously implicated in itch, but which couples to the inhibition of adenylate cyclase [37] and may therefore inhibit neuronal activity. Experiments were carried out on DRG from control Avil^{iDTR} mice and Sst-Cre::Avil^{iDTR} mice, both treated systemically with diphtheria toxin. Application of histamine to cells evoked a characteristic phasic calcium response in approximately 10% of neurons from control mice, which upon ablation was reduced to less than 1% (Fig 6H and L). Chloroquine and IL-31 activated a similar number of neurons in control mice with a corresponding decrease in the number of responsive cells in DRG from Sst-Cre::Avil^{iDTR} mice (Fig 6I, J and L). Finally, we examined the function of the $5HT_{1F}$ receptor by applying the $5HT_{1F}$ agonist LY344864 to neurons. Unexpectedly, we found that application of low concentrations of LY344864 evoked calcium flux in a small population of neurons that was also reduced upon ablation of Sst^{Cre} neurons (Fig 6K and L). In all cases, responses to pruritogens which remained after ablation were quantitatively similar to those from control cultures (Fig EV4).

The Avil^{iDTR} strategy opens up the possibility to determine how ablation of the Sst^{Cre} population impacts upon mouse behavior, and thus translate *in vitro* observations in DRG to events occurring in sensory neuron endings in the skin. To explore this, we first examined nociceptive thresholds in control Avil^{iDTR} and Sst-Cre::Avil^{iDTR} mice treated with diphtheria toxin. We observed no significant difference in thermal withdrawal thresholds in the hot plate test ($P = 0.17$, Fig 7A) or mechanical thresholds to calibrated von Frey filaments ($P = 0.32$, Fig 7B). We next considered responses to pruritogens by quantifying scratching behavior after intradermal injection of agonists tested in isolated DRG. We first assayed responses in control (Avil^{iDTR}) and Sst-Cre::Avil^{iDTR} mice in the absence of diphtheria toxin. All compounds including the $5HT_{1F}$ agonist LY344864 evoked robust scratching behavior compared to vehicle (Figs 7C–F and EV5). We then applied diphtheria toxin systemically to these mice and reexamined scratching responses. Strikingly, we observed a significant reduction in scratching behavior in Sst-Cre::Avil^{iDTR} mice evoked by IL-31 and LY344864, but not by histamine or chloroquine (Figs 7C–F and EV5). Responses in control Avil^{iDTR} mice were not influenced by diphtheria toxin application, indicating that Sst^{Cre} neurons (and thus the Ret-eGFP^{Lo}:IB4^{Neg} population) mediate itch sensation *in vivo*.

Discussion

Here, we show that a previously uncharacterized population of sensory neurons that express the receptor tyrosine kinase Ret function as itch receptors. Using flow cytometry of dissociated DRG neurons, we isolated this population based upon its weak expression of Ret and absence of IB4 binding. We demonstrate that these neurons express markers such as TrkA and Sst, and importantly are highly enriched for transcripts associated with itch sensation. Anatomical and functional analysis of these cells indicates that they form a rare subtype of DRG neuron and function to detect itch inducing stimuli.

Three populations of Ret-positive sensory neuron have been previously identified and characterized. Early Ret neurons develop

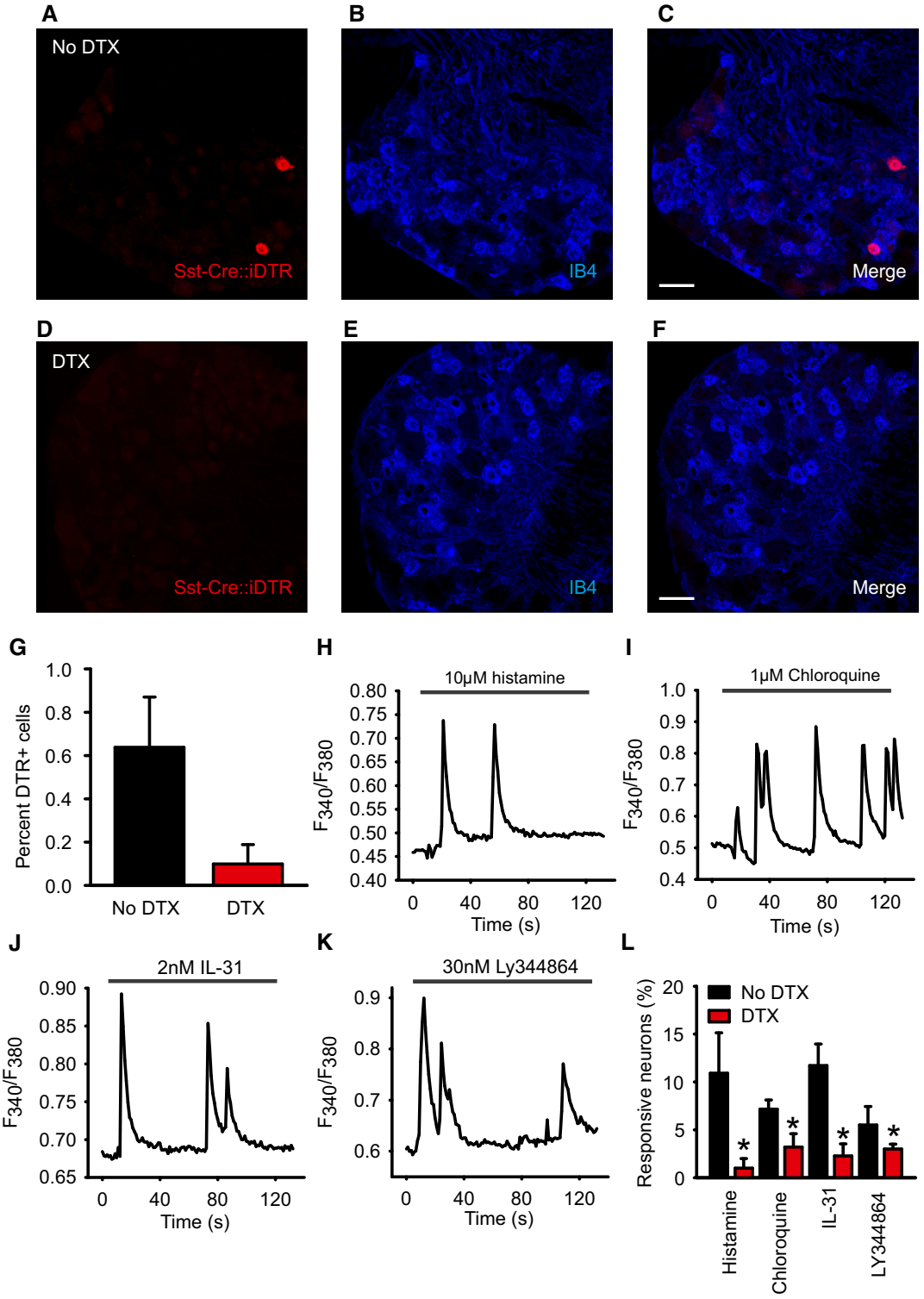

Figure 6. Diphtheria toxin-mediated ablation of Sst^{Cre}-positive DRG neurons.

A–G Ablation of Sst-Cre::Avil^{iDTR}-positive sensory neurons by injection of diphtheria toxin (DTX). Immunostaining of DRG from Sst-Cre::Avil^{iDTR} mice with an antibody against the diphtheria toxin receptor and IB4 in the absence of diphtheria toxin (A–C) and after systemic injection of diphtheria toxin (D–F). (G) Quantification of diphtheria toxin receptor-positive neurons before and after injection of diphtheria toxin.

H–K Examples of calcium flux in dissociated DRG upon application of histamine (H), chloroquine (I), IL-31 (J), and 5HT$_{1F}$ agonist Ly344864 (K).

L Quantification of percent responding neurons to the indicated pruritogens before or after systemic injection of diphtheria toxin in Sst-Cre::Avil^{iDTR} mice.

Data information: Scale bars, 50 μm. Asterisk denotes $P < 0.05$, $n = 4$–6 mice, Student's t-test, error bars indicate SEM.

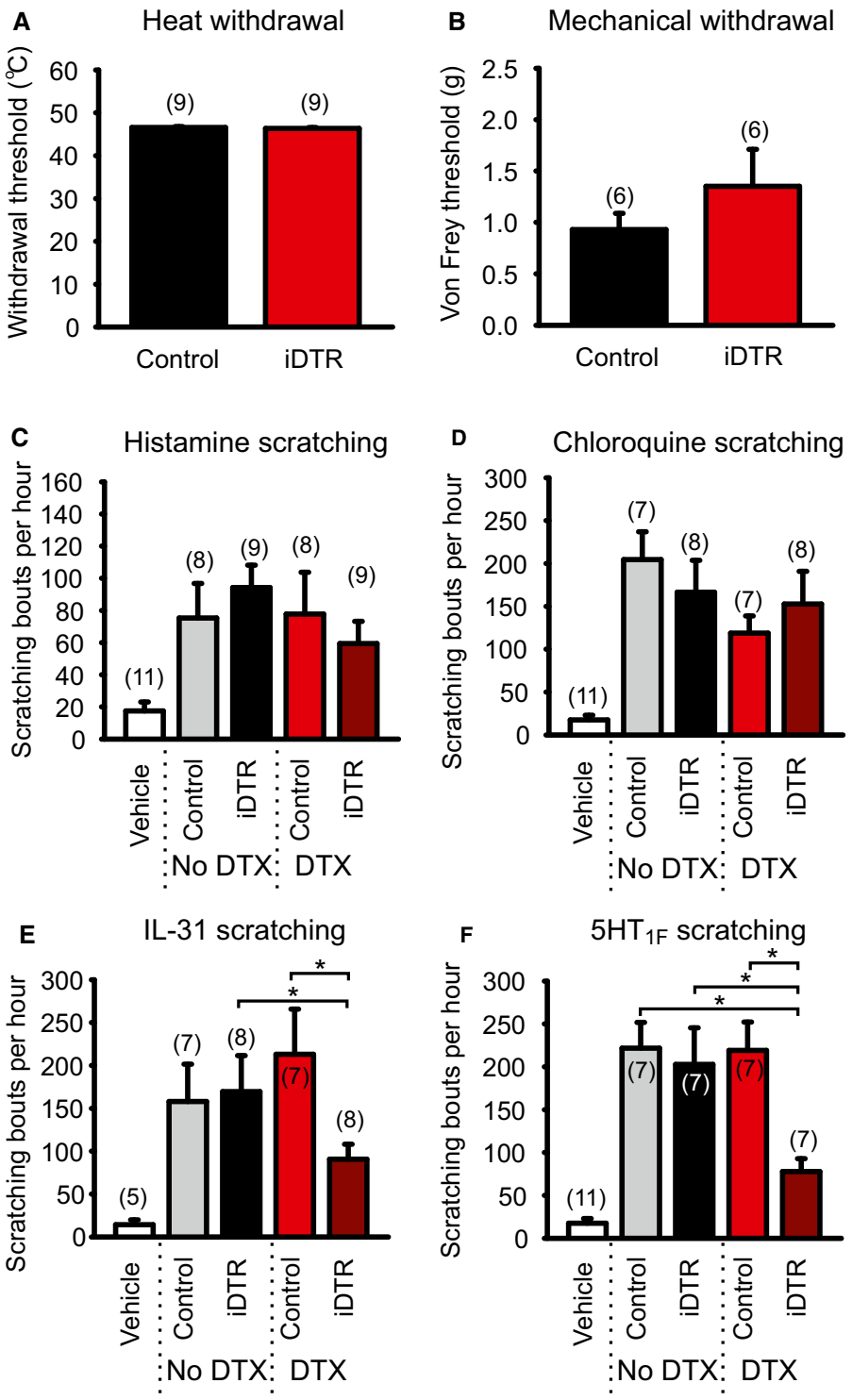

Figure 7. Reduced scratching behavior in Sst-Cre::Avil^{iDTR} mice after diphtheria toxin-mediated ablation.

A, B Nociceptive withdrawal thresholds in control (Avil^{iDTR} without the Cre) and Sst-Cre::Avil^{iDTR} mice after systemic diphtheria toxin injection. No significant differences in thermal (A) or mechanical (B) withdrawal reflexes after ablation of Sst^{Cre}-positive neurons.

C–F Scratching behavior after a single intradermal injection of the indicated pruritogen observed for 1 h. All compounds evoked a significant increase in the number of scratching bouts compared to vehicle alone in control (Avil^{iDTR}) or Sst-Cre::Avil^{iDTR} mice. Diphtheria toxin injection in control mice (Avil^{iDTR}) had no effect on scratching behavior evoked by histamine (C), chloroquine (D), IL-31 (E), or 5HT$_{1F}$ agonist Ly344864 (F) but significantly reduced responses to IL-31 or Ly344864 in Sst-Cre::Avil^{iDTR} mice.

Data information: *n* numbers indicated in brackets, and asterisk denotes $P < 0.05$, two-way RM ANOVA, Holm–Sidak multiple comparison. Error bars indicate SEM.

into RA mechanoreceptors [25,26], while late Ret neurons become C-fiber low threshold mechanoreceptors and non-peptidergic nociceptors [22,28]. Intriguingly, a fourth population of Ret-positive neurons has also been described that expresses TrkA in adult mice but has unknown function [22,30]. This population is scarce, corresponding to around 10% of all Ret-positive cells [22,30], and presumably this rarity has made further analysis difficult. By taking advantage of the sensitivity and analytic power of flow cytometry, we have isolated these cells and performed gene expression profiling to determine their function.

We initially used histochemistry to identify populations of Ret-eGFP-positive neuron expressing markers of mechanoreceptors (NF200), non-peptidergic nociceptors (IB4), and C-fiber low threshold mechanoreceptors (TH). However, limited by the number of markers that can be applied simultaneously to the same section, we turned to flow cytometry to analyze Ret expression in more detail. We based our analysis on the observation that Ret expression levels differ considerably across the DRG and that low Ret levels correlate with GFRα1/3 expression [24], while high Ret-expressing neurons express GFRα2 and form RA mechanoreceptors [25,26]. By co-labeling cells with IB4, we were able to distinguish multiple subtypes of Ret-positive neurons of which a Ret-low, IB4-negative population was clearly evident. That this population corresponds to the fourth, uncharacterized type of Ret neuron is supported by several lines of evidence. Firstly, it is IB4 negative, indicating that it is not part of the non-peptidergic nociceptor population. Secondly, it expresses almost 10-fold less Ret transcript compared to Ret-eGFP^{Hi}:IB4^{Neg} neurons. Thirdly, Gfra3 is upregulated 29-fold in these cells, while Gfra2 has 21-fold higher expression in the Ret-eGFP^{Hi}:IB4^{Neg} population. Finally, we detected many differentially expressed genes such as TrkA, CGRP, and TRPV1, in the Ret-eGFP^{Lo}:IB4^{Neg} population which are known to be absent from C-LTMRs or RA mechanoreceptors [28]. While we did not perform a similar analysis on IB4-positive neurons, flow cytometry data indicate that further three populations can also be differentiated here which may also form distinct functional populations.

Given the powerful regulatory actions of neurotrophic factors in the peripheral nervous system, a major emphasis of previous research has been to investigate how deletion of these factors impacts upon the survival, differentiation, and maintenance of distinct populations. Here, we have not considered the effects of Ret ablation on Ret-eGFP^{Lo}:IB4^{Neg}-negative neurons, concentrating instead upon the initial functional characterization of this population. Of note, the number of Ret-positive/TrkA-positive neurons is not reduced in Ret nociceptor-specific conditional knockout mice [30], suggesting that this population does not require Ret for its survival. It is, however, possible that the termination pattern of these neurons in the skin and spinal cord, and the expression of ion channels and signaling molecules are regulated by Ret signaling as has been shown for other populations [22,24–28,30,38]. The identification of markers and molecular tools with which to target Ret-eGFP^{Lo}:IB4^{Neg}-negative cells described here would now allow for further investigation of these phenotypes.

Among the differentially expressed genes present in Ret-eGFP^{Lo}:IB4^{Neg} cells, we observed a strong enrichment of the neuropeptides CGRP, Nppb, neurotensin (Nts), and somatostatin (Sst). Of these, we focused our attention on Sst because of the availability of an Sst-Cre driver line [34] which we reasoned could be used to target the Ret-eGFP^{Lo}:IB4^{Neg} population. Indeed, recombination of the *Ret* or *Rosa26* locus by Sst-Cre occurred in very few neurons of the DRG, resulting in fluorescence in mainly IB4- and NF200-negative cells, analogous to the Ret-eGFP^{Lo}:IB4^{Neg} population. Moreover, flow cytometry analysis and transcriptional profiling revealed that these neurons overlap. Of note, Sst-Cre-mediated recombination of eGFP and RFP reporters resulted in a lower number of positive cells when compared to the Ret-eGFP^{Lo}:IB4^{Neg} population, or to antibody staining of Sst. We suggest that this may be due to the lower sensitivity of reporter fluorophores [35]. Indeed, in ablation experiments which require minimal expression of the diphtheria toxin receptor to induce cell death, we observed around 10% reduction in the number of cells responding to pruritogens such as histamine.

To define the function of the Sst-Cre/Ret-eGFP^{Lo}:IB4^{Neg} population, we generated a new mouse line which allows for selective ablation of Cre-positive sensory neurons regardless of whether Cre recombinase is expressed in other tissues beyond the DRG. Using this mouse, we were able to selectively ablate Sst-positive neurons and found that both cellular and behavioral responses to pruritogens but not nociceptive behavior were reduced upon ablation. Intriguingly, we also observed several differences between *in vitro* studies on isolated DRG and *in vivo* studies examining scratching behavior. For example, histamine- and chloroquine-evoked responses were sensitive to diphtheria toxin ablation in isolated DRG, but were not affected at the whole animal level. One possible explanation for this discrepancy is that ablation of Sst-Cre-positive neurons does indeed eliminate those neurons which respond directly to the tested pruritogens. However, *in vivo*, alternative pathways involving other cell types may be evoked (especially by histamine and chloroquine) which in turn activate a broader spectrum of neurons to trigger scratching. It was also unexpected that scratching behavior was only partially reduced *in vivo*. Indeed, knockout mice for Nbbp show an almost complete loss of itch-evoked behavior [3], and Nbbp was highly upregulated in Ret-eGFP^{Lo}:IB4^{Neg} neurons and is co-expressed with Sst [29,30]. Since our data indicate that Sst neurons are fully ablated upon treatment with diphtheria toxin (Fig EV4), this would suggest that Nbbp is also expressed outside of the Sst population. Thus, the Avil^{iDTR} mouse line may be a useful tool for establishing functional overlap between different populations of sensory neuron.

We were intrigued by the high expression levels of the serotonin receptors Htr1f and Htr1a in Ret-eGFP^{Lo}:IB4^{Neg} neurons. Serotonin has a well-established pruritogenic action when applied subcutaneously and this effect is mediated by 5-HT$_2$ receptors [40,41]. Transcripts for 5-HT$_2$ receptors were not upregulated in Ret-eGFP^{Lo}:IB4^{Neg} cells and we did not investigate further whether serotonin directly activates these cells. Instead, we focused on the 5HT$_{1F}$ receptor because it is coupled to G$_i$ signaling and should therefore inhibit neuronal activation. Unexpectedly, we observed an apparent activation of Ret-eGFP/IB4-negative sensory neurons by the 5HT$_{1F}$ agonist LY344864 and robust scratching behavior when LY344864 was injected intradermally in control animals. A potential basis for this effect may come from the observation that many G$_i$-coupled receptors are able to interact with G$_{14}$ subunits promoting the stimulation of phospholipase C [42]. Indeed, the transcript for G$_{14}$ (Gna14) was among the most differentially expressed genes in Ret-eGFP^{Lo}:IB4^{Neg} neurons (Fig 5A–C), and thus, its presence could expand the signaling repertoire of these cells allowing for G$_i$-coupled

receptors such as $5HT_{1F}$ to generate neuronal activity. Of note, $5HT_{1F}$ receptor agonists have also been proposed as clinical targets for the treatment of migraine [43]. Our data indicate that these compounds could have unwanted side effects via activation of Sst-Cre/Ret-eGFP^{Lo}:IB4^{Neg} neurons and generation of itch.

In addition to the four pruritogen receptors examined here, many molecules previously implicated in itch sensation such as Cysltr2, Plcb3, and Nppb were enriched in the Ret-eGFP^{Lo}:IB4^{Neg} population. However, other itch-associated transcripts were absent from the transcriptome data including GRP, MrgprC11, endothelin receptors, and TSLP receptor transcripts (Il7r and Crlf2) which play a critical role in the development of atopic dermatitis [44]. These data support the recent finding that several populations of putative itch receptors exist in the mouse which may be tuned to selectively detect the multitude of irritants which can evoke scratching behavior [20]. Our data on the expression profile of Ret-eGFP^{Lo}:IB4^{Neg} neurons provide a molecular inventory for one of these populations, and as such many more molecules with an as yet unexplored role in itch may be contained within this list. Moreover, this complexity suggests that therapeutic strategies for treating itch should target common signaling molecules or disrupt neuronal function, rather than inhibit specific receptors. The transcriptional profiling approach described here is a first step toward identifying these molecules.

Materials and Methods

Transgenic mouse lines

To study Ret expression in adult primary sensory neurons, we crossed RET$^{eGFP/+}$ [31] mice with the DRG neuron-specific Cre line Avil$^{cre/+}$ [32] to obtain Avil-Cre::RET$^{eGFP/+}$ mice. We also used the Avil$^{cre/+}$ line to mark sensory neurons within the DRG by crossing it with a Rosa26^{tdRFP} strain [45] to generate Avil-Cre::R26$^{tdRFP/+}$ mice. To specifically mark Ret-eGFP^{Lo}:IB4^{Neg} neurons, we bred Sst$^{cre/+}$ [34] and RET$^{eGFP/+}$ mice, thus obtaining Sst-Cre::Ret$^{eGFP/+}$ animals. To mark all Sst-positive neurons, we crossed the Sst^{Cre} line with the above-mentioned Rosa26^{tdRFP} strain, generating Sst-Cre::R26$^{tdRFP/+}$ mice. To visualize Sst-positive nerve endings, the Sst$^{Cre/+}$ mice were bred with Rosa26$^{SnapCaaX/+}$ animals [35] to obtain Sst-Cre::Rosa26$^{SnapCaaX/+}$ offspring.

To ablate Sst-positive sensory neurons, we crossed the Sst^{Cre} line with an Avil^{iDTR} line, thus obtaining Sst-Cre::Avil$^{iDTR/+}$ mice that express the diphtheria toxin receptor specifically in Sst-positive DRG neurons.

The Avil^{iDTR} line was obtained by classical knock-in of the iDTR cassette Lox-STOP-Lox-DTR (kindly provided by the Waisman group in Mainz) into the *Avil* locus, to replace exon 2 and 66 bp upstream thereof (Fig EV3). The targeting construct was transfected into A9 ES cells. Individual ES cell clones underwent Southern blot screening to identify homologous recombinants. DNA was digested with PstI and HindIII and hybridized with 5′ or 3′ probe, respectively, obtaining 9,600 (wild-type)- and 6,300 (targeted)-bp DNA fragments by using the 5′ probe and 7,100 (wild-type)- and 5,600 (targeted)-bp DNA fragments by using the 3′ probe. Positive clones were injected into 8-cell stage embryos to generate mice heterozygous for the targeted allele. To assess mouse genotype, PCR was performed with the following primers: aggagcgagggctcagttgggctgt (forward) and acaccaggttagcctttaagcctgc (reverse) for the wild-type and ctgccacccaggttaccatggagagagg (forward) and cattctagttgtggtttgtc caaactca (reverse) for the mutant allele, giving PCR products of 313 and 287 bp, respectively. Heterozygous mice were all viable and exhibited no overt behavioral phenotype.

All mice were bred and maintained at the EMBL Mouse Biology Unit, Monterotondo, in accordance with Italian legislation (Art. 9, 27. Jan 1992, no 116) under license from the Italian Ministry of Health, and in compliance with the ARRIVE guidelines. The Avil^{iDTR} conditional allele has been deposited in the European Mutant Mouse Archive (www.emmanet.org).

Immunofluorescence

DRG and spinal cord from adult mice (6 weeks or older) were post-fixed in 4% PFA for 30 min (DRG) or 2 h (SC), embedded in 12% bovine gelatin, and sectioned using a vibratome at 50–100 μm. Sections were incubated for 30 min in 50% ethanol and then overnight in 0.3% Triton X-100, and 5% goat or donkey serum in PBS at 4°C containing one or more antibodies diluted as shown below. Secondary antibodies and streptavidin-647 were diluted (1:1,000 and 1:600, respectively) in 0.3% Triton X-100, 5% goat or donkey serum in PBS and left for 1–2 h at 4°C. Slides were mounted with Prolong gold antifade (Invitrogen, P36930).

For immunofluorescence analysis of the Avil-Cre::RET$^{eGFP/+}$ mouse skin, the hair was removed and skin collected and postfixed in 4% PFA for 8–12 h, incubated in 30% sucrose overnight, and frozen in OCT. 35-μm sections were cut with a cryostat. Antibody staining was performed as described above.

For SNAP-tag analysis of the Sst-Cre::Rosa26$^{SnapCaaX/+}$ mouse peripheral nerve endings, the back skin of the animals was injected intradermally with 10 μM of Snap-Cell TMR-Star (New England Biolabs, S9105S). After 6 h, the skin was collected and treated as described above. Once sectioned, the skin was additionally stained with DAPI (Invitrogen, D1306).

We used the following primary antibody dilutions: mouse anti-NF200 (Sigma Aldrich, N0142) 1:500, goat anti-CGRP (Santa Cruz, SC8856) 1:500, rabbit anti-PKCγ (Santa Cruz, SC-211) 1:100, isolectin GS-B4-biotin XX conjugate (Invitrogen I21414) 1:100, rabbit anti-RFP (Rockland, 600-401-379) 1:200, rabbit anti-TH (Millipore, AB152) 1:1,000, rabbit anti-PGP9.5 antibody (Dako, Z5116) 1:200.

To visualize the cells expressing the diphtheria toxin receptor, we used goat anti-human HB-EGF antibody (R&D Systems, AF-259-NA).

Sst, NF200, and IB4 staining was performed on acutely dissociated neurons from Sst-Cre::Avil$^{iDTR/+}$ and control Avil$^{iDTR/+}$ (without the Cre), after treatment with diphtheria toxin. Cells were dissociated with 1 mg/ml collagenase IV and 0.05% trypsin (Gibco, 25300-054) for 25 min each at 37°C and subsequently plated on glass coverslips treated with poly-L-lysine. Cells were fixed with 4% PFA for 5 min and permeabilized 10 min with 0.1% Triton X-100/PBS. Blocking with 3% normal goat serum in 0.01% Tween-20/PBS was performed for 20 min and cells were then stained overnight at 4°C with rat anti-Sst (1:50 concentration, MAB354, Millipore), mouse anti-NF200 (1:1,000), and IB4 (1:100). After washing with PBS, secondary antibody staining was performed for 1.5 h. Glass coverslips were then mounted with Prolong gold antifade.

All images were visualized with a Leica SP5 confocal microscope and analyzed with ImageJ.

Flow cytometry and microarray analysis

To quantitatively analyze the distribution of Ret^+ sensory neurons in DRG, we used flow cytometry on Avil-Cre::$RET^{eGFP/+}$ mice: DRG were collected from 10 adult Avil-Cre::$RET^{eGFP/+}$ mice (6 weeks or older) and pooled. Cells were dissociated with 1 mg/ml collagenase IV and 0.05% trypsin (Gibco, 25300-054) for 25 min each at 37°C and subsequently kept on ice in 1% FBS in PBS. Cells were labeled in suspension with 1:50 anti-mouse CD16/32 (eBioscience 14-0161-85) for 5 min and isolectin GS-B4-biotin XX conjugate (1:100) for 10 min. After washing, cells were incubated immediately with a cocktail containing streptavidin-Alexa 647 and anti-CD45-PeCy7 for 5 min, washed, and resuspended in 1% FBS in PBS.

To isolate the whole sensory neuron population, we applied flow cytometric analysis and subsequent sorting on Avil-Cre::$R26^{tdRFP/+}$ mice: DRG were collected from three adult Avil-Cre::$R26^{tdRFP/+}$ mice (6 weeks or older) and pooled. Cell dissociation was performed as described above. Cells were then labeled in suspension with 1:50 anti-mouse CD16/32 (eBioscience 14-0161-85) for 5 min, and after washing, cells were incubated in anti-CD45-PeCy7 (1:200) for 5 min, washed, and resuspended in 1% FBS in PBS.

To analyze the distribution of Ret- and Sst-positive sensory neurons, we used flow cytometry on Sst-Cre::$Ret^{eGFP/+}$ animals. Sensory neurons from 10 mice were collected, isolated, and stained following the same protocol used for the analysis of Avil-Cre::$RET^{eGFP/+}$ mice.

Flow cytometric online and offline analyses were performed in a FACS Aria III SORP (BD Bioscience) using FACS Diva software (BD Bioscience) and FlowJo (Tree Star, Inc.), respectively. For gene expression analysis, DRG cells were sorted (see Fig EV1) using an 85-μm nozzle (40 PSI) directly into RLT buffer (RNeasy kit, Qiagen) and RNA was purified according to manufacturer instructions. Two rounds of RNA amplification, labeling, and hybridization to Affymetrix® MOE430 2.0 GeneChip® expression arrays were performed by the EMBL Gene Core Facility. Microarray data were analyzed as detailed in the Appendix. All data have been submitted to ArrayExpress with the accession code E-MTAB-1836.

Fluidigm

To validate the microarray data, we used the microfluidic platform Fluidigm to perform quantitative RT–PCR. DRG from Avil-Cre::$RET^{eGFP/+}$ mice were collected and processed as described above. Cells were sorted directly into 5 μl of CellsDirect (Invitrogen, PN 11753-100 and 11753-500) 2× Buffer, and combined with 0.2 μl of RT/Taq mix, 1 μl of assay pool (formed by 38 individual assay pairs that were previously pooled and diluted to a final concentration of 500 nM), and 2.8 μl of water. The samples went through target-specific RT and pre-amplification (16 cycles) following manufacturer instructions. Pre-amplified cDNA was then diluted 1:10 and combined together with 2.5 μl 2× SsoFast Evagreen Supermix (Bio-Rad, PN 172-5211) and 0.25 μl 20× Sample Loading Reagent (Fluidigm, PN 100-0388) and loaded onto the sample inlets of a 48.48 Fluidigm Dynamic Array. All 38 individual assays pairs (100 μM) were diluted by combining 0.25 μl of each assay with 2.25 μl of TE Buffer (TEKnova, PN T0224) and 2.5 μl of Assay Loading Reagent (Fluidigm, PN 85000736). The 48.48 chip was then loaded on the IFC Controller MX and 30 cycles of qPCR were performed on the Fluidigm BioMark HD system. Data were analyzed using Fluidigm Real-Time Analysis Software.

To compare the level of expression of the 38 genes between Ret-$eGFP^{Lo}$:$IB4^{Neg.}$- and Sst-Cre::Ret^{eGFP}-positive sensory neurons, we used Fluidigm platform to perform qRT–PCR on DRG neurons sorted from Sst-Cre::$Ret^{eGFP/+}$ animals. We followed the same procedure described above.

qRT–PCR

DRG were dissected from adult Sst-Cre::$Avil^{iDTR/+}$ and control $Avil^{iDTR/+}$ (without the Cre) mice treated with 40 μg/kg of diphtheria toxin (2 injections, the second injection occurring 72 h after the first one). Mice were sacrificed 8 days after the second DTX injection. RNA was isolated using Trizol and reverse-transcribed using Superscript II (Invitrogen). Quantitative RT–PCR was then performed with LightCycler 480 SYBR Green I Master kit (Roche, 04707516001) following manufacturer instructions and using Roche LightCycler 480 instrument. The expression of each gene was calculated relatively to ubiquitin using the $2^{-\Delta\Delta Ct}$ method.

Calcium imaging

DRG from adult Sst-Cre::$Avil^{iDTR/+}$ and control $Avil^{iDTR/+}$ (without the Cre) mice were collected and incubated in 1 mg/ml collagenase IV (Sigma Aldrich, C5138) and 0.05% trypsin (Gibco, 25300-054) for 25 min each at 37°C. They were then suspended in DRG medium (DMEM (Gibco, 41966-029) with the addition of 10% heat inactivated FBS (PAA, A15101), 0,8% glucose and 100 U of penicillin/streptomycin (Gibco, 15140-122)). Cells were plated in a droplet of medium on glass coverslips treated with poly-L-lysine and left to attach for 3 h at 37°C.

Cells were then incubated in 3 μM Fura2-AM (Invitrogen, F1221) in CIB (140 mM NaCl, 4 mM KCl, 2 mM $CaCl_2$, 1 mM $MgCl_2$, 4.55 mM NaOH, 5 mM glucose, 10 mM HEPES, pH 7.4) and calcium imaging was performed as described [46]. Concentrations of compounds used were as follows: histamine, 1 μM (Sigma, H7250); LY344864, 30 nM (Abcam, ab120592); IL-31, 2 nM (Peprotech, 210-31); chloroquine, 500 μM (Sigma, C 6628).

Behavior

To evaluate the scratching response of animals prior and after ablation of the Sst-positive sensory neurons, we removed the hair of the neck of 6- to 8-week-old Sst-Cre::$Avil^{iDTR/+}$ and control $Avil^{iDTR/+}$ mice with an electric shaver. The animals were acclimatized for 2–3 days and the following day they were injected intradermally with 50 μl solution in the nape of the neck with one of the following reagents: 10 mM histamine (Sigma, H7250) in saline, 1 mM LY344864 (Abcam, ab120592) in saline, 5.6 μM IL-31 (Peprotech, 210-31) in 0.1% BSA/PBS, 12.5 mM chloroquine (Sigma, C 6628) in saline. Control injections were performed with appropriate vehicle. Animals were observed for 60 min and bouts of scratching counted.

One bout was defined as an event of scratching lasting from when the animal lifted the hind paw to scratch until it returned it to the floor or started licking it.

The actual time of scratching was also assessed, considered as the time from when the animal started scratching until it put its hind paw down.

The same animals were then injected i.p. with 40 μg/kg of DTX (Sigma D0564). After 72 h, a second injection of DTX was performed. After 5 days, mice were again acclimatized for 2–3 days, and at the 8th day after the second DTX injection, scratching behavior was assessed again, using the same reagent of the first test, at the same concentration.

For the hot plate and the von Frey tests, Sst-Cre::Avil$^{iDTR/+}$ and Avil$^{iDTR/+}$ (without the Cre) mice were injected twice with 40 μg/kg of DTX, with the second injection occurring 72 h after the first one. The tests were performed 8 days after the second DTX injection, after 2–3 days of acclimatization.

For the hot plate test, each animal was placed on the hot plate (Ugo Basile) and left to acclimatize for 30 min. A gradient from 42 to 49°C was applied and stopped as soon as a paw withdrawal or licking was observed. This was repeated for 2–3 days. On the day of the actual test, animals were placed again on the hot plate and the gradient was applied: The temperature at which a paw withdrawal or licking was observed was registered as individual threshold for thermal nociception.

For the von Frey test, animals were acclimatized by placing them in cages on a mesh platform and by applying von Frey filaments (North Coast Medical) on the plantar surface of the hind paw. The actual test was performed following the simplified up–down method proposed by Bonin *et al* [47].

Sample sizes were determined from the power of the statistical test performed. No animals were excluded and all experiments were performed blinded with order of testing randomized.

Expanded View for this article is available online.

Acknowledgements
We thank Dr. Sanjay Jain for providing us with the RET$^{eGFP/+}$ mice, Dr. Ari Waisman for supplying the iDTR cassette for the Adv-iDTR mouse, Paul Collier and the EMBL Genomics Core Facility for Fluidigm and Microarray procedures, Maria Kamber and the EMBL Monterotondo Mouse Phenotyping, Giulia Bolasco and the Microscopy facility for technical support of our work, and Violetta Paribeni and Stefano Tatti for mouse husbandry.

Author contributions
The study was designed by PAH and KKS. KKS, LI, RD, CM, LC, LN, EP, CP, MP, KSS, FCR, and DB performed experiments and TP performed bioinformatics analysis. PAH wrote the paper with contributions from other authors.

Conflict of interest
The authors declare that they have no conflict of interest.

References

1. Ma Q (2010) Labeled lines meet and talk: population coding of somatic sensations. *J Clin Invest* 120: 3773 – 3778
2. Han L, Ma C, Liu Q, Weng HJ, Cui Y, Tang Z, Kim Y, Nie H, Qu L, Patel KN *et al* (2013) A subpopulation of nociceptors specifically linked to itch. *Nat Neurosci* 16: 174 – 182
3. Mishra SK, Hoon MA (2013) The cells and circuitry for itch responses in mice. *Science* 340: 968 – 971
4. Sun YG, Zhao ZQ, Meng XL, Yin J, Liu XY, Chen ZF (2009) Cellular basis of itch sensation. *Science* 325: 1531 – 1534
5. Ikoma A, Steinhoff M, Stander S, Yosipovitch G, Schmelz M (2006) The neurobiology of itch. *Nat Rev Neurosci* 7: 535 – 547
6. Schmelz M, Schmidt R, Weidner C, Hilliges M, Torebjork HE, Handwerker HO (2003) Chemical response pattern of different classes of C-nociceptors to pruritogens and algogens. *J Neurophysiol* 89: 2441 – 2448
7. Schmelz M, Schmidt R, Bickel A, Handwerker HO, Torebjork HE (1997) Specific C-receptors for itch in human skin. *J Neurosci* 17: 8003 – 8008
8. Davidson S, Zhang X, Yoon CH, Khasabov SG, Simone DA, Giesler GJ Jr (2007) The itch-producing agents histamine and cowhage activate separate populations of primate spinothalamic tract neurons. *J Neurosci* 27: 10007 – 10014
9. Imamachi N, Park GH, Lee H, Anderson DJ, Simon MI, Basbaum AI, Han SK (2009) TRPV1-expressing primary afferents generate behavioral responses to pruritogens via multiple mechanisms. *Proc Natl Acad Sci USA* 106: 11330 – 11335
10. Han SK, Mancino V, Simon MI (2006) Phospholipase Cbeta 3 mediates the scratching response activated by the histamine H1 receptor on C-fiber nociceptive neurons. *Neuron* 52: 691 – 703
11. Yosipovitch G, Papoiu AD (2008) What causes itch in atopic dermatitis? *Curr Allergy Asthma Rep* 8: 306 – 311
12. Ajayi AA, Oluokun A, Sofowora O, Akinleye A, Ajayi AT (1989) Epidemiology of antimalarial-induced pruritus in Africans. *Eur J Clin Pharmacol* 37: 539 – 540
13. Liu Q, Tang Z, Surdenikova L, Kim S, Patel KN, Kim A, Ru F, Guan Y, Weng HJ, Geng Y *et al* (2009) Sensory neuron-specific GPCR Mrgprs are itch receptors mediating chloroquine-induced pruritus. *Cell* 139: 1353 – 1365
14. Wilson SR, Gerhold KA, Bifolck-Fisher A, Liu Q, Patel KN, Dong X, Bautista DM (2011) TRPA1 is required for histamine-independent, Mas-related G protein-coupled receptor-mediated itch. *Nat Neurosci* 14: 595 – 602
15. Liu T, Ji RR (2012) Oxidative stress induces itch via activation of transient receptor potential subtype ankyrin 1 in mice. *Neurosci Bull* 28: 145 – 154
16. Fernandes ES, Vong CT, Quek S, Cheong J, Awal S, Gentry C, Aubdool AA, Liang L, Bodkin JV, Bevan S *et al* (2013) Superoxide generation and leukocyte accumulation: key elements in the mediation of leukotriene B (4)-induced itch by transient receptor potential ankyrin 1 and transient receptor potential vanilloid 1. *FASEB J* 27: 1664 – 1673
17. Akiyama T, Carstens E (2013) Neural processing of itch. *Neuroscience* 250: 697 – 714
18. Cevikbas F, Wang X, Akiyama T, Kempkes C, Savinko T, Antal A, Kukova G, Buhl T, Ikoma A, Buddenkotte J *et al* (2013) A sensory neuron-expressed IL-31 receptor mediates T helper cell-dependent itch: Involvement of TRPV1 and TRPA1. *J Allergy Clin Immunol* 133: 448 – 460
19. Dillon SR, Sprecher C, Hammond A, Bilsborough J, Rosenfeld-Franklin M, Presnell SR, Haugen HS, Maurer M, Harder B, Johnston J *et al* (2004) Interleukin 31, a cytokine produced by activated T cells, induces dermatitis in mice. *Nat Immunol* 5: 752 – 760

20. Usoskin D, Furlan A, Islam S, Abdo H, Lonnerberg P, Lou D, Hjerling-Leffler J, Haeggstrom J, Kharchenko O, Kharchenko PV *et al* (2015) Unbiased classification of sensory neuron types by large-scale single-cell RNA sequencing. *Nat Neurosci* 18: 145 – 153
21. Marmigere F, Ernfors P (2007) Specification and connectivity of neuronal subtypes in the sensory lineage. *Nat Rev Neurosci* 8: 114 – 127
22. Molliver DC, Wright DE, Leitner ML, Parsadanian AS, Doster K, Wen D, Yan Q, Snider WD (1997) IB4-binding DRG neurons switch from NGF to GDNF dependence in early postnatal life. *Neuron* 19: 849 – 861
23. Airaksinen MS, Saarma M (2002) The GDNF family: signalling, biological functions and therapeutic value. *Nat Rev Neurosci* 3: 383 – 394
24. Luo W, Wickramasinghe SR, Savitt JM, Griffin JW, Dawson TM, Ginty DD (2007) A hierarchical NGF signaling cascade controls Ret-dependent and Ret-independent events during development of nonpeptidergic DRG neurons. *Neuron* 54: 739 – 754
25. Luo W, Enomoto H, Rice FL, Milbrandt J, Ginty DD (2009) Molecular identification of rapidly adapting mechanoreceptors and their developmental dependence on ret signaling. *Neuron* 64: 841 – 856
26. Bourane S, Garces A, Venteo S, Pattyn A, Hubert T, Fichard A, Puech S, Boukhaddaoui H, Baudet C, Takahashi S *et al* (2009) Low-threshold mechanoreceptor subtypes selectively express MafA and are specified by Ret signaling. *Neuron* 64: 857 – 870
27. Franck MC, Stenqvist A, Li L, Hao J, Usoskin D, Xu X, Wiesenfeld-Hallin Z, Ernfors P (2011) Essential role of Ret for defining non-peptidergic nociceptor phenotypes and functions in the adult mouse. *Eur J Neurosci* 33: 1385 – 1400
28. Li L, Rutlin M, Abraira VE, Cassidy C, Kus L, Gong S, Jankowski MP, Luo W, Heintz N, Koerber HR *et al* (2011) The functional organization of cutaneous low-threshold mechanosensory neurons. *Cell* 147: 1615 – 1627
29. Olausson H, Wessberg J, Morrison I, McGlone F, Vallbo A (2010) The neurophysiology of unmyelinated tactile afferents. *Neurosci Biobehav Rev* 34: 185 – 191
30. Golden JP, Hoshi M, Nassar MA, Enomoto H, Wood JN, Milbrandt J, Gereau RWt, Johnson EM Jr, Jain S (2010) RET signaling is required for survival and normal function of nonpeptidergic nociceptors. *J Neurosci* 30: 3983 – 3994
31. Jain S, Golden JP, Wozniak D, Pehek E, Johnson EM Jr, Milbrandt J (2006) RET is dispensable for maintenance of midbrain dopaminergic neurons in adult mice. *J Neurosci* 26: 11230 – 11238
32. Zurborg S, Piszczek A, Martinez C, Hublitz P, Al Banchaabouchi M, Moreira P, Perlas E, Heppenstall PA (2011) Generation and characterization of an Advillin-Cre driver mouse line. *Mol Pain* 7: 66
33. Jensen RT, Battey JF, Spindel ER, Benya RV (2008) International Union of Pharmacology. LXVIII. Mammalian bombesin receptors: nomenclature, distribution, pharmacology, signaling, and functions in normal and disease states. *Pharmacol Rev* 60: 1 – 42
34. Taniguchi H, He M, Wu P, Kim S, Paik R, Sugino K, Kvitsiani D, Fu Y, Lu J, Lin Y *et al* (2011) A resource of Cre driver lines for genetic targeting of GABAergic neurons in cerebral cortex. *Neuron* 71: 995 – 1013
35. Yang G, de Castro Reis F, Sundukova M, Pimpinella S, Asaro A, Castaldi L, Batti L, Bilbao D, Reymond L, Johnsson K *et al* (2015) Genetic targeting of chemical indicators *in vivo*. *Nat Methods* 12: 137 – 139
36. Buch T, Heppner FL, Tertilt C, Heinen TJ, Kremer M, Wunderlich FT, Jung S, Waisman A (2005) A Cre-inducible diphtheria toxin receptor mediates cell lineage ablation after toxin administration. *Nat Methods* 2: 419 – 426
37. Adham N, Kao HT, Schecter LE, Bard J, Olsen M, Urquhart D, Durkin M, Hartig PR, Weinshank RL, Branchek TA (1993) Cloning of another human serotonin receptor (5-HT1F): a fifth 5-HT1 receptor subtype coupled to the inhibition of adenylate cyclase. *Proc Natl Acad Sci USA* 90: 408 – 412
38. Honma Y, Kawano M, Kohsaka S, Ogawa M (2010) Axonal projections of mechanoreceptive dorsal root ganglion neurons depend on Ret. *Development* 137: 2319 – 2328
39. Li CL, Li KC, Wu D, Chen Y, Luo H, Zhao JR, Wang SS, Sun MM, Lu YJ, Zhong YQ *et al* (2016) Somatosensory neuron types identified by high-coverage single-cell RNA-sequencing and functional heterogeneity. *Cell Res* 26: 83 – 102
40. Yamaguchi T, Nagasawa T, Satoh M, Kuraishi Y (1999) Itch-associated response induced by intradermal serotonin through 5-HT2 receptors in mice. *Neurosci Res* 35: 77 – 83
41. Nojima H, Carstens E (2003) 5-Hydroxytryptamine (5-HT)2 receptor involvement in acute 5-HT-evoked scratching but not in allergic pruritus induced by dinitrofluorobenzene in rats. *J Pharmacol Exp Ther* 306: 245 – 252
42. Ho MK, Yung LY, Chan JS, Chan JH, Wong CS, Wong YH (2001) Galpha (14) links a variety of G(i)- and G(s)-coupled receptors to the stimulation of phospholipase C. *Br J Pharmacol* 132: 1431 – 1440
43. Goadsby PJ (2005) New targets in the acute treatment of headache. *Curr Opin Neurol* 18: 283 – 288
44. Wilson SR, The L, Batia LM, Beattie K, Katibah GE, McClain SP, Pellegrino M, Estandian DM, Bautista DM (2013) The epithelial cell-derived atopic dermatitis cytokine TSLP activates neurons to induce itch. *Cell* 155: 285 – 295
45. Luche H, Weber O, Nageswara Rao T, Blum C, Fehling HJ (2007) Faithful activation of an extra-bright red fluorescent protein in "knock-in" Cre-reporter mice ideally suited for lineage tracing studies. *Eur J Immunol* 37: 43 – 53
46. Caspani O, Zurborg S, Labuz D, Heppenstall PA (2009) The contribution of TRPM8 and TRPA1 channels to cold allodynia and neuropathic pain. *PLoS One* 4: e7383
47. Bonin RP, Bories C, De Koninck Y (2014) A simplified up-down method (SUDO) for measuring mechanical nociception in rodents using von Frey filaments. *Mol Pain* 10: 26

